Structural and Functional Regulation of Tight Junctions by RhoA and Rac1 Small GTPases

Tzuu-Shuh Jou,* Eveline E. Schneeberger,‡ and W. James Nelson*

*Department of Molecular and Cellular Physiology, Stanford University School of Medicine, Stanford, CA 94305-5345;
‡Department of Pathology, Massachusetts General Hospital, Boston, MA 02114

Abstract. Tight junctions (TJ) govern ion and solute diffusion through the paracellular space (gate function), and restrict mixing of membrane proteins and lipids between membrane domains (fence function) of polarized epithelial cells. We examined roles of the RhoA and Rac1 GTPases in regulating TJ structure and function in MDCK cells using the tetracycline repressible transactivator to regulate RhoAV14, RhoAN19, Rac1V12, and Rac1N17 expression. Both constitutively active and dominant negative RhoA or Rac1 perturbed TJ gate function (transepithelial electrical resistance, tracer diffusion) in a dose-dependent and reversible manner. Freeze-fracture EM and immunofluoresence microscopy revealed abnormal TJ strand morphology and protein (occludin, ZO-1) localization in RhoAV14 and Rac1V12 cells. However, TJ strand morphology and protein localization appeared normal in RhoAN19 and Rac1N17 cells. All mutant GTPases disrupted the fence function of the TJ (interdomain diffusion of a fluorescent lipid), but targeting and organization of a membrane protein in the apical membrane were unaffected. Expression levels and protein complexes of occludin and ZO-1 appeared normal in all mutant cells, although ZO-1 was more readily solubilized from RhoAV14-expressing cells with Triton X-100. These results show that RhoA and Rac1 regulate gate and fence functions of the TJ, and play a role in the spatial organization of TJ proteins at the apex of the lateral membrane.

Key words: GTPase • RhoA • epithelial cells • tight junction • polarity

EPITHELIA form barriers and regulate vectorial transport of ions and solutes between different biological compartments separated by these barriers, thereby contributing to the maintenance of homeostasis (Almers and Stirling, 1984). Two key structural features of transporting epithelial cells specify this function: restricted distributions of specific membrane proteins to functionally distinct membrane domains that face these compartments (Rodriguez-Boulan and Nelson, 1989), and formation of an intercellular junctional complex (Farquhar and Palade, 1963). The tight junction (TJ),[1] the most apical structure of the junctional complex, acts as a selective permeability barrier to the paracellular space (gate function; Diamond, 1977), and an intramembranous fence to prevent free mixing of membrane domain-specific proteins and lipids (fence function; Dragsten et al., 1981; van Meer et al., 1986; van Meer and Simons, 1986).

Address all correspondence to W. James Nelson, Department of Molecular and Cellular Physiology, Stanford University School of Medicine, Beckman Center, B121, Stanford, CA 94305-5345. Tel.: 650-725-7596; Fax: 650-498-5286; E-mail: wjnelson@leland.stanford.edu

1. *Abbreviations used in this paper*: DC, doxycycline; TER, transepithelial electrical resistance; TJ, tight junctions.

The TJ has a well-described but poorly understood structure. Freeze-fracture EM has depicted the TJ as a continuous network of parallel and interconnected strands that circumscribe the apex of lateral membranes of adjacent cells (Claude, 1978). Early studies sought to establish a relationship between TJ strand number and function (Claude, 1978), but it has been difficult to extrapolate generalizations to all cell types (Stevenson et al., 1988). Little is known about how TJ functions are regulated in different physiological or pathological conditions, or about the molecular basis for differences in the paracellular permeability of leaky (e.g., proximal renal tubule) and tight epithelia (e.g., distal renal tubule).

The protein composition and organization of TJ are being uncovered. Occludin is the only TJ transmembrane protein identified so far (Furuse et al., 1993). Immunoelectron microscopy combined with freeze fracture has shown that occludin is localized to TJ strands (Fujimoto, 1995). Overexpressing full-length occludin or mutant occludin lacking the cytoplasmic domain (Balda et al., 1996; McCarthy et al., 1996), or adding a synthetic peptide corresponding to the second extracellular loop of occludin (Wong and Gumbiner, 1997) perturb TJ gate function. However, recent evidence from transgenic ablation of the

© The Rockefeller University Press, 0021-9525/98/07/101/15 $2.00

occludin gene indicates that occludin is not required for TJ gate function (Saitou et al., 1998). Note, however, that ectopic expression of occludin in fibroblasts confers cell–cell adhesion, indicating that occludin has some adhesive function in TJ organization (van Itallie and Anderson, 1997).

Several cytoplasmic proteins interact either directly or indirectly with occludin, including ZO-1 and ZO-2 (Itoh et al., 1993; Willott et al., 1993; Jesaitis and Goodenough, 1994; Furuse et al., 1994). These proteins may act as a protein scaffold to organize occludin at the TJ. For example, the spatial organization of occludin on the membrane of fibroblasts requires coexpression of ZO-1 (van Itallie and Anderson, 1997). ZO-1 and ZO-2 also contain PDZ domain and SH3 domains (Fanning and Anderson, 1996; Itoh et al., 1993; Jesaitis and Goodenough, 1994; Songyang et al., 1997; Willott et al., 1993), and may recruit signaling molecules and the actin cytoskeleton to the TJ.

A number of signaling molecules have been implicated in the regulation of TJ function, including tyrosine kinases, cAMP, Ca^{2+}, protein kinase C, heterotrimeric G proteins, and phospholipase C (Anderson and van Itallie, 1995; Cereijido et al., 1993). Two targets common to these molecules are actin (Anderson and van Itallie, 1995) and the perijunctional actin–myosin ring located subjacent to the apical junction complex (Madara, 1988). It has been proposed that contraction of peri-junctional actin filaments and the resulting centrifugal traction on TJ membrane regulates TJ permeability (Madara et al., 1988).

Signaling molecules that directly control actin cytoskeleton organization are particularly intriguing with regard to TJ function regulation. The family of Ras-related small GTP-binding proteins RhoA, Rac1, and Cdc42 are regulators of the actin cytoskeleton (Hall, 1998). Microinjection of RhoA, Rac1, or Cdc42 induces stress fiber formation, membrane ruffling, and extension of filopodia, respectively, in serum-starved Swiss 3T3 fibroblasts (Ridley and Hall, 1992; Ridley et al., 1992). Recent studies have implicated RhoA GTPases in TJ functions. Nusrat et al. (1995) found that the organization of the perijunctional actin cytoskeleton and ZO-1 were disrupted after exposing T84 cells to recombinant *Clostridium botulinum* exotoxin C3, which ADP-ribosylates Rho family proteins and disrupts their functions (Aktories, et al., 1989; Sekine et al., 1989). Concomitantly, the TJ gate function was disturbed. Nusrat et al. (1995) also transiently expressed RhoC in T84 cells and observed a condensation of actin filament at cell–cell contact sites, but a functional analysis of TJ was not reported. Takaishi et al. (1997) examined MDCK cells constitutively expressing RhoA mutant genes, and reported no effect on the TJ morphology at steady state except during PKC-induced TJ assembly in the presence of low extracellular calcium concentrations, but they did not perform ultrastructural or functional analyses of the TJ.

To study roles of RhoA and Rac1 in the structural and functional organization of TJ, we generated MDCK cells that express RhoA and Rac1 mutants under the control of the tetracycline repressible transactivator (Gossen and Bujard, 1992). As shown in the preceding study (Jou and Nelson, 1998), this system has advantages over constitutive gene expression and protein microinjection. Functional analysis of TJ in these mutants revealed that the gate function was disrupted upon expression of RhoA and Rac1 mutants in a dose-dependent and reversible manner. Constitutively active RhoA and Rac1 mutants induced a dramatic disorganization of TJ strands and protein (occludin, ZO-1, actin) distribution, while dominant negative RhoA and Rac1 mutants affected neither TJ morphology nor TJ protein distribution. All mutants disrupted TJ fence function, as determined by interdomain diffusion of a fluorescent membrane lipid, but targeted delivery and membranous distribution of an apical membrane protein from the TGN were unaffected. This analysis of TJ structure and function in the presence of different RhoA mutants, coupled with the ability to examine the same cell population without mutant protein expression, provides new insights into the roles of RhoA GTPases in controlling TJ assembly, dynamics, and function.

Materials and Methods

Cell Culture

T23 MDCK cells expressing RhoAV14, RhoAN19, Rac1V12, or Rac1N17 under control of the tetracycline-repressible transactivator were described in detail in the preceding study (Jou and Nelson, 1998). Parental T23 cells and transfected cells were grown in DMEM containing 10% FBS and 20 ng/ml doxycycline (DC; Sigma Chemical Co., St Louis, MO) at 37°C in a humidified atmosphere containing 5% CO_2. Cultures were routinely monitored for Mycoplasma infection. Generally, mutant genes were induced to express for 16–18 h (RhoAV14, Rac1V12, Rac1N17) or 40 h (RhoAN19) by removing DC (Sigma Chemical Co.) from the culture medium before each experiment. In calcium-switch experiments, control and mutant small GTPase-expressing cells were grown in the presence or absence of 20 ng/ml DC at low density, trypsinized, and plated onto 12-mm–diameter Transwell™ filters (Corning Costar Corp., Cambridge, MA) in medium containing 5 μM calcium (LCM) with or without 20ng/ml DC (Nelson and Veshnock, 1987). Cells were incubated in LCM for 4 h, gently rinsed in prewarmed LCM twice, and then incubated in DMEM/FBS containing 1.8 mM calcium (HCM) with or without 20 ng/ml DC.

Adenovirus-mediated Expression of $p75^{NTR}$

cDNA encoding a receptor for nerve growth factor ($p75^{NTR}$) was introduced into polarized MDCK cells by adenovirus-mediated gene transfer (Yeaman, et al., 1997). Replication-defective adenovirus vector encoding $p75^{NTR}$ (AdCMVp75) was kindly provided by Dr. Moses Chao (Cornell University Medical College, New York). Recombinant adenovirus were applied to the apical surface of MDCK cells grown on Transwell™ filters in serum-free DMEM for 2 hr. After infection, DMEM/FBS was added and cells were incubated at 37°C for 24 h.

Antibodies

The following antibodies were used: rabbit polyclonal anti-occludin antibody (Zymed Laboratories, Inc., South San Francisco, CA), rabbit polyclonal anti-myc antibody (Santa Cruz Biotechnology, Inc., Santa Cruz, CA), rabbit polyclonal anti-ZO-2 antibody (no. 9989) and rat anti-ZO-1 hybridoma R40.76 (Dr. D.A. Goodenough, Harvard Medical School, Cambridge, MA), mouse anti-myc hybridoma 9E10 (Dr. Gordon Cann, Stanford Univ. Med. Sch., Stanford, CA), mouse anti-p75 monoclonal antibody (Dr. C. Yeaman, Stanford University, Stanford, CA), and affinity-purified fluorescein and rhodamine-labeled secondary antibodies (Jackson ImmunoResearch Laboratories, Inc., West Grove, PA).

Transepithelial Electrical Resistance (TER) Measurement

TER was determined by applying an AC square wave current of ± 20 mA at 12.5 Hz across a cell monolayer on a 12-mm–diameter Transwell™ filter, and measuring the voltage deflection with a pair of Ag/AgCl voltage sensors (EVOM, World Precision Instruments). TER values were calculated by subtracting the blank values from the filter and the bathing me-

dium, and were normalized to the area of the monolayer (filter). Monolayer integrity was monitored after each TER time course study by staining cells with Hoechst 33342 (Molecular Probes, Inc., Eugene, OR).

Measurement of Paracellular Diffusion of Nonionic Molecular Tracers

Paracellular flux assays were performed on confluent monolayers of MDCK cells grown on rat tail collagen-coated polycarbonate Transwell™ filters (0.4-μm pore size, 12-mm diameter). Three different tracers were used: [^{3}H]inulin (Amersham Corp., Arlington Heights, IL), anionic dextran (mol wt 3,000) conjugated with FITC (Molecular Probes, Inc.), and neutral dextran (mol wt 40,000) conjugated with Texas Red (Molecular Probes, Inc.). The assay was begun by replacing the apical compartment medium with 200 μl DMEM containing one of the tracers (4 nM inulin, 0.2 mg/ml FITC-conjugated dextran [mol wt 3,000], or 0.5 mg/ml Texas Red–conjugated dextran [mol wt 40,000]); basal compartment medium was replaced with 600 μl DMEM/FBS without tracer. Cells were incubated at 37°C for either 30 min (inulin) or 3 h (3K and 40K dextrans), and then equal-volume aliquots of apical and basal compartment media were collected, and the amount of [^{3}H]inulin or 3K or 40K dextrans was determined in a scintillation counter or a fluorometer (Fluoroskan II™; K & M Co., Torrance, CA), respectively. The amount of diffusible inulin or dextran was calculated from a titration curve of known concentrations of the tracer.

Freeze-fracture EM

Monolayers of cells grown in 75-cm^2 plastic tissue culture flasks (Becton Dickinson, Franklin Lakes, NJ) or on 10 cm–diameter Transwell™ filters were fixed in 0.1 M phosphate buffer, pH 7.4 containing 2% glutaraldehyde for 30 min at room temperature. After rinsing in phosphate buffer, cells were removed from the substratum using a plastic cell scraper (Nunc Inc., Naperville IL). The detached cells were infiltrated with 25% glycerol in 0.1 M cacodylate buffer, pH 7.3, frozen in a liquid nitrogen slush, and freeze-fractured in a Balzers 400 freeze fracture unit (Balzers, Liechtenstein). Replicas were cleaned in sodium hypochlorite, washed in distilled water, placed on Formvar-coated grids, and examined in a 301 electron microscope (Philips, Eindhoven, Netherlands).

In a given replica, all grid squares were examined, and all TJ images were photographed. The number of TJ parallel strands was measured on electron micrographs by overlaying the area of the TJ with a transparency marked at 1-cm intervals. Since the magnification on all micrographs examined was 62,500×, measurements were effectively made at 160-nm intervals. Total TJ length examined by morphometry in each group ranged from 49 to 79 μm. When histograms were constructed for the strand frequency, the strand counts were normalized to the shortest total length measured. Note that the strand distribution in the apical and lateral membranes, and the frequently interrupted pattern of TJ strands in RhoAV14-expressing cells complicated strand counting. Morphometric data were analyzed as a parallel electrical circuit as described (Madara and Dharmsathaphorn, 1985). All freeze-fracture experiments were performed and analyzed as a double-blind study.

Immunofluorescence Microscopy

Confluent monolayers of MDCK cells were grown on rat tail collagen-coated coverslips or Transwell™ filters in DMEM/FBS with or without 20 ng/ml DC. Cells were washed twice with Dulbecco's PBS (0.9 mM $CaCl_2$, 2.7 mM KCl, 1.5 mM KH_2PO_4, 0.5 mM $MgCl_2$, 137 mM NaCl, and 8.1 mM Na_2HPO_4) and then fixed for 20 min at room temperature in 3.7% paraformaldehyde in Dulbecco's PBS. Cells were then washed twice in Dulbecco's PBS at room temperature for 10 min and extracted with CSK buffer (50 mM NaCl, 300 mM sucrose, 10 mM Pipes, pH 6.8, 3 mM $MgCl_2$, 0.5% [vol/vol] Triton X-100) at room temperature for 10 min. Cells were washed twice in Dulbecco's PBS at room temperature for 10 min. Cells were blocked in Dulbecco's PBS containing 1% BSA, 10% goat serum, and 50 mM NH_4Cl for 1 h at room temperature, or overnight at 4°C. After blocking, cells were washed briefly in Dulbecco's PBS and 0.2% BSA, and then incubated in primary antibody solution for 1 h at room temperature or overnight at 4°C. Cells were then washed three times in Dulbecco's PBS and 0.2% BSA, and incubated in fluorescein- or rhodamine-conjugated goat secondary antibody solution for 1 h at room temperature. Cells were washed three times in Dulbecco's PBS and 0.2% BSA, and were mounted in either Elvanol (16.7% Mowiol, 33% glycerol, 0.1% phenylenediamine), or Vectashield™ (Vector Laboratories, Inc., Burlingame, CA). Cells were viewed with an Axioplan™ epifluorescence microscope (Carl Zeiss, Inc., Thornwood, NY) using either a 40× or 63× oil immersion objective. Alternatively, cells were viewed using a laser scanning confocal microscope MultiProbe 2010 (Molecular Dynamics, Sunnyvale, CA). Fluorescent images of stained cells were recorded using Ektachrome Elite II (ASA 400; Eastman Kodak Co., Rochester, NY) film. Photographic images were then digitized with a slide scanner (Nikon, Inc., Melville, NY) and images were resized, arranged, and labeled using Adobe Photoshop software (Adobe, Mountain View, CA). The resulting images were printed from the computer file using a dye sublimation printer (Tektronix Inc., Beaverton, OR). The images are representative of the original data.

Fluorescent Lipid Labeling of the Plasma Membrane

BODIPY-FL-C_5 sphingomyelin (Molecular Probes. Inc.) and defatted BSA (Boehringer Mannheim Corp., Indianapolis, IN) were used to prepare sphingomyelin/BSA complexes (5 nmol/ml) in *P* buffer (10 mM Hepes, pH 7.4, 1 mM sodium pyruvate, 10 mM glucose, 3 mM $CaCl_2$, and 145 mM NaCl). Duplicate confluent monolayers of MDCK cells grown on Transwell™ filters (12-mm diameter, 0.4-μm pore size) were used for fluorescent lipid labeling. Before labeling, cells were washed twice in prechilled *P* buffer, and then 0.5 ml 5 μM sphingomyelin/BSA complex solution was added to the apical compartment while 1 ml *P* buffer was added to the basal compartment. The incubation was performed for 10 min on ice, and then both apical and basal compartment solutions were removed and saved for further analysis. Filters were washed three times in cold *P* buffer. One filter was immediately processed for confocal microscopy, and the other filter was washed extensively in *P* buffer and then left on ice in *P* buffer containing BSA for 1 h before confocal microscopy. 100 μl of solution was collected from the apical and basal medium after the initial incubation, and was used to assess paracellular leakage of BSA/lipid complex between filter compartments.

Immunoblotting

MDCK cells were grown on Transwell™ filters and extracted in 900 μl Triton X-100 extraction buffer (0.5% [vol/vol] Triton X-100, 10 mM Tris-HCl, pH 7.5, 120 mM NaCl, 25 mM KCl, and 1.8 mM $CaCl_2$) containing 25 mg/ml pepstatin A, 1 mM Pefabloc, 1 mM benzamidine, 1% aprotinin, 100 mM leupeptin, 1 mM sodium vanadate, and 50 mM NaF on a rocker platform for 10 min at 4°C. Cells were scraped from the filter using a rubber policeman, and were centrifuged at 12,000 *g* for 15 min at 4°C; pellets were dissolved in 100 μl SDS-IP buffer (1% SDS, 10 mM Tris-HCl, pH 7.5, 2 mM EDTA) at 100°C, and were then diluted with 900 μl Triton X-100 extraction buffer; supernatants were adjusted with 100 μl SDS-IP buffer. Protein concentrations in supernatants and pellets were determined using the BCA protein assay reagent kit (Pierce Chemical Co., Rockford, IL). Equal amounts of total protein (reconstituted by adding supernatant and pellet fraction from each sample) or supernatant or pellet were separated either in 5% (for ZO-1 and ZO-2) or 7.5% (for occludin) SDS-PAGE, transferred electrophoretically to nitrocellulose filters, and processed for immunoblotting with specific antibodies to occludin, ZO-1, or ZO-2. Immune complexes were visualized with donkey anti–rabbit and sheep anti–rat horseradish peroxidase–conjugated secondary antibodies (Amersham Corp.) and developed using the ECL kit (Amersham Corp.). Chemiluminescent signals were collected and scanned from autoradiography film (Eastman Kodak Co.) into Adobe Photoshop software (Adobe, Mountain View, CA) with a Scan-Jet IIc™ scanner (Hewlett-Packard Co., Greeley, CO). The contrast of images was adjusted, arranged, and labeled for individual figures in Adobe Photoshop. The resulting images were printed using a dye sublimation printer (Tektronix, Inc.). The printed images are representative of the original data. Intensities of signals were measured with National Institutes of Health Image 1.58 software.

Results

RhoA and Rac1 Mutants Disrupt TJ Gate Function: Transepithelial Resistance

The effects of mutant small GTPases on TJ function were examined in MDCK cells after induction of cell–cell contact. Different amounts of constitutively active or dominant negative RhoA or Rac1 were expressed by varying the con-

centration of DC in the medium (20 ng/ml –0 pg/ml) as reported in the previous study; these data are not shown again here, but the reader is referred to the data in Figs. 1 and 3 in Jou and Nelson (1998).

TER of each mutant cell line was measured at different times over a 24-h period after induction of cell–cell contacts (see Materials and Methods). TER increased linearly in control cells (T23 and pUHD10-3), reached 200–250 ohms per cm^2 after 24 h, and was not affected by different concentrations of DC (Fig. 1). In contrast, cells expressing RhoA or Rac1 mutants showed a dose-dependent effect of mutant protein on TER (RhoAV14, RhoAN19, Rac1V12, and Rac1N17). In general, cells expressing RhoA or Rac1 mutants grown in the presence of 20 ng/ml DC developed TER with kinetics similar to that of controls; at this DC concentration, RhoA and Rac1 mutants were not expressed (Jou and Nelson, 1998). In the presence of 200 pg/ml DC, cells expressing Rac1V12 and Rac1N17 developed slightly lower than normal TER, but in cells expressing RhoAV14 or RhoAN19, TER developed very poorly (Fig. 1); at this DC concentration, we detected very low levels of RhoAV14, but levels of Rac1V12, Rac1N17, and RhoAN19 were below that detectable by Western blotting of whole cell extracts (Jou and Nelson, 1998). At concentrations of DC at or below 20 pg/ml, TER in all mutants developed poorly to levels that were only 10–20% of that of parental cells or mutant cells in which mutant gene expression was fully repressed. At 20 pg/ml DC, proteins were expressed at 20% (Rac1V12), 50% (Rac1N17), 46% (RhoAV14) and 13% (RhoAN19) of the respective endogenous wild-type Rac1 or RhoA levels; in the absence of DC, proteins were expressed at 104% (Rac1V12), 600% (Rac1N17), 200% (RhoAV14) or 60% (RhoAN19) of the respective endogenous wild-type Rac1 or RhoA levels (see Figs. 1 and 3 in Jou and Nelson, 1998). Note that TER values obtained in cells fully expressing RhoA or Rac1 mutants, while low compared with the levels for control cells, were still significantly higher than those reported in some leaky epithelial cells. This result indicates that in these mutants some TJ structure may be preserved, providing a minimal barrier function to paracellular ion flow.

Differences in TER sensitivity to the expression of RhoA or Rac1 mutants were unlikely to be due to different kinetics of gene induction. At 20 pg/ml DC, both RhoAV14 and RhoAN19 expression were induced to ~50% of the level of endogenous RhoA (Jou and Nelson, 1998), but RhoAV14 had a more profound effect on TER than did RhoAN19. At 20 pg/ml DC, the level of Rac1V12 protein was similar to that of endogenous Rac1 while Rac1N17 was induced to level >5× that of endogenous Rac1 protein, and yet Rac1V12 suppressed TER development more than Rac1N17. These results indicate that RhoAV14 and Rac1V12 have different regulatory effect(s) on TJ structure and function than RhoAN19 or Rac1N17.

RhoA and Rac1 Mutants Disrupt TJ Gate Function: Nonionic Molecules

In addition to regulating paracellular ion flow (measured by TER), the TJ also regulates diffusion of nonionic molecules through the paracellular space. We examined the effects of RhoA or Rac1 mutants on the diffusion of three nonionic tracers: [^{3}H]inulin (mol wt 5,200), FITC-conjugated dextran (mol wt 3,000), and Texas Red–conjugated dextran (mol wt 40,000; Fig. 2). Tracer diffusion was examined 18 h after induction of cell–cell contacts in confluent monolayers of MDCK cells in which RhoA or Rac1 mutant expression was either completely repressed (20 ng/ml

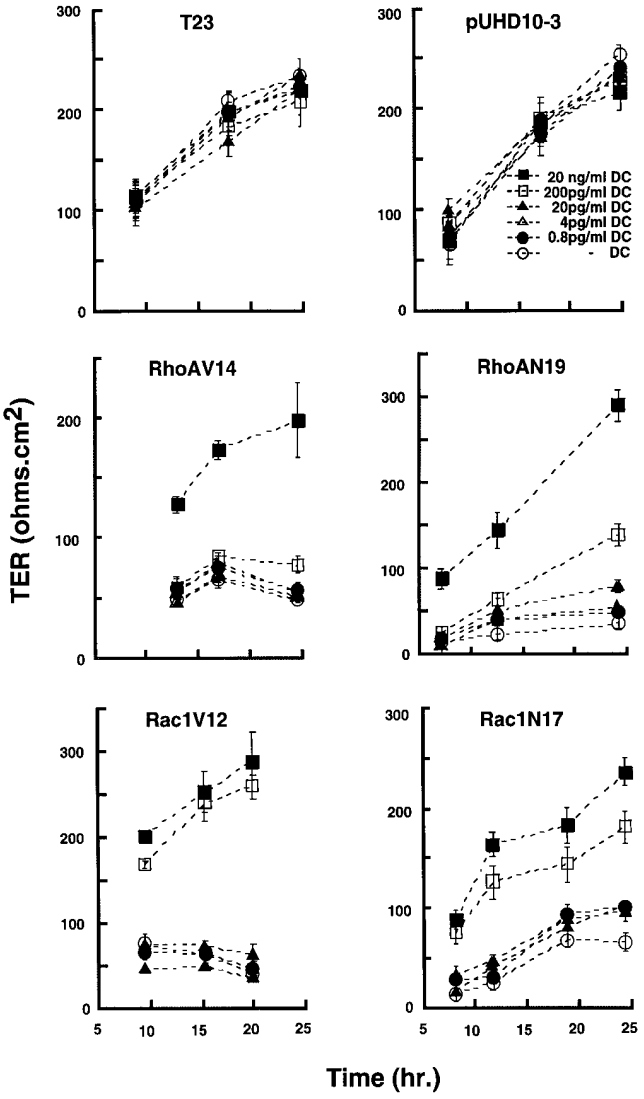

Figure 1. Development of TER in MDCK cells expressing constitutively active or dominant negative RhoA or Rac1 mutants. Control MDCK cells (*T23*), mock-transfected MDCK cells (*pUHD10-3*), and cells expressing RhoAV14, RhoAN19, Rac1V12, or Rac1N17 under control of the tetracycline repressible transactivator were grown in different concentrations of DC for 16 h at low cell density. Cells were trypsinized, plated on Transwell™ filters as an instant confluent monolayer in LCM containing different amounts of DC for 4 h, and then cell–cell contacts were synchronously induced by switching to HCM containing different amounts of DC. TER (ohms per cm^2) was measured at different times after induction of cell–cell contacts (see Materials and Methods). TER was measured in four filters for each cell line and each DC concentration, and the data are reported as the mean ± SEM. At the end of the experiment, filters were fixed and stained with Hoechst 33342 (Molecular Probes, Inc.) to check the integrity of each monolayer.

DC) or maximal (absence of DC). In control cells (T23, pUHD), in the absence or presence of DC, minimal amounts of [^{3}H]inulin, 3K, and 40K dextran diffused through the paracellular space (Fig. 2). All cell lines in which RhoA or Rac1 mutant expression was repressed (+DC) also blocked tracer diffusion to levels similar to those in controls (Fig. 2). However, expression of RhoAV14, RhoAN19, Rac1V12, or Rac1N17 caused a two- to sevenfold increase in paracellular permeability to [^{3}H]inulin, an 8- to 12-fold increase in permeability to 3K dextran, and a 7- to 40-fold increase in permeability to 40K dextran compared with controls (Fig. 2). Of the RhoA or Rac1 mutants examined, RhoAV14 was the most effective in disrupting TJ size selectivity to all of the tracers tested, even though its expression level was only slightly higher than those of RhoAN19 and Rac1V12, and was considerably lower than that of Rac1N17 (see above; Jou and Nelson, 1998). The other RhoA or Rac1 mutants were approximately equally effective in disrupting the diffusion barrier to the low–molecular weight tracers [^{3}H]inulin and 3K dextran (Fig. 2). However, there was a progressive increase in potency of these mutants (Rac1N17 > Rac1V12 > RhoAN19) to disrupt the barrier to 40K dextran (Fig. 2). Taken together, we conclude that the TJ gate function is disrupted in the presence of all mutant GTPases.

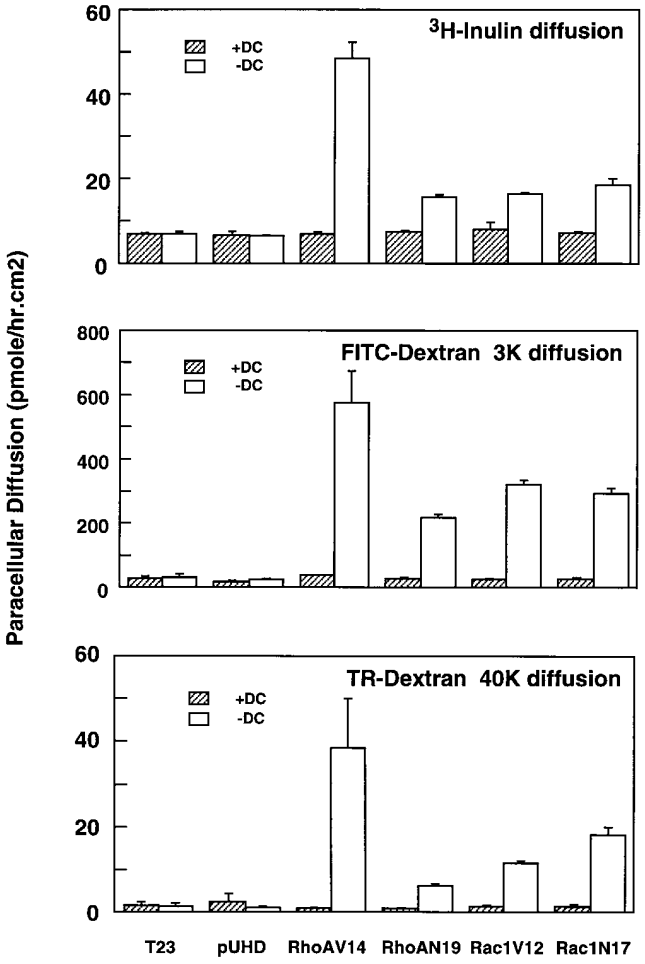

Figure 2. RhoA and Rac1 mutants disrupt TJ barrier to paracellular diffusion of [^{3}H]inulin, FITC-conjugated 3K dextran, and Texas Red–conjugated 40K dextran. Control MDCK cells (*T23*), mock-transfected MDCK cells (*pUHD*), and cells expressing RhoAV14, RhoAN19, Rac1V12, or Rac1N17 under the control of the tetracycline repressible transactivator, were cultured with 20 ng/ml DC or without DC at low cell density. Cells were trypsinized and plated on Transwell™ filters at an instant confluent monolayer density in LCM (± DC) for 4 h, and were then switched to normal DMEM/FBS (± DC). 16 h later, paracellular tracer diffusion was measured in four parallel cultures for each cell line ± DC as described in Materials and Methods; the data are shown as the mean ± SEM.

RhoA and Rac1 Mutants Disrupt TJ Strand Organization

Freeze-fracture EM of TJs in epithelial cells has revealed a fine interconnected network of parallel strands and cross-

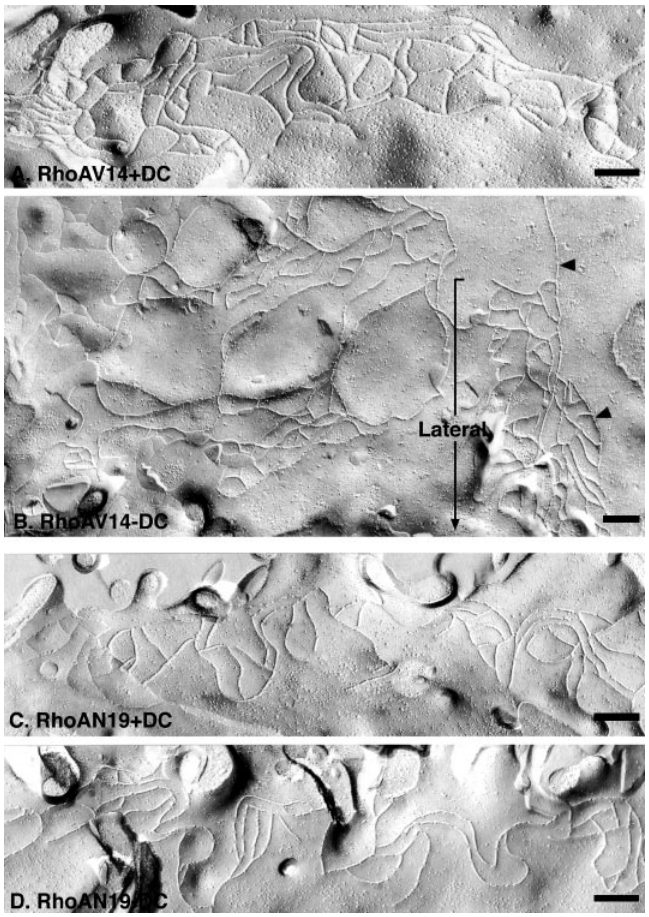

Figure 3. Freeze-fracture EM of tight junction strand organization in MDCK cells expressing RhoA mutants. (*A* and *B*) Representative *P* fracture face of a TJ from MDCK cells expressing RhoAV14 +DC (*A*) or −DC (*B*). Fracture planes are oriented with the apical membrane at the top (from left to right), and lateral membranes are oriented downwards (*bracket*). Note the chaotically distributed TJ strands that extend basally from a disorganized TJ (*arrowheads*) in RhoAV14 -DC cells (*B*). (*C* and *D*) Representative *P* fracture face of a TJ from MDCK cells expressing RhoAN19 +DC (*C*) or −DC (*D*). The strand organization of the TJs in RhoAN19 +DC or −DC are similar. Bars, 200 nm.

bridges (Staehelin, 1974). Although the molecular organization of proteins in these strands is poorly understood, strand organization provides a measure of TJ integrity (Claude, 1978). As expected from previous studies, freeze-fracture analysis of the TJ region of control MDCK cells (+DC) revealed a number of parallel strands and cross-bridges that were restricted to the apex at the lateral membranes (Fig. 3, *A* and *C,* and Fig. 4, *A* and *C*; mutant + DC); these images are similar to those described previously for MDCK cells (Stevenson et al., 1988).

Compared with the TJ strand organization in control cells, freeze-fracture analysis of cells expressing RhoAV14 revealed a chaotic disorganized arrangement of strands at the apical surface (Fig. 3 *B*); some regions of the membrane were devoid of strands (which contributed to the overall decrease in strand number [Fig. 5]), while others contained multiple strands that interwove with each other rather than forming parallel lines with cross-bridges (Fig. 3 *B*). Significantly, we also found strands that extended from the apical membrane down the lateral membrane to the base of the cell (Fig. 3 *B*). In contrast to the constitutively active mutant, RhoAN19 expressing cells had a TJ ultrastructure similar to that of control cells (Fig. 3 *D*). Strand number and organization of parallel strands in cells expressing Rac1N17 also appeared similar to that in control cells, although we detected a slight decrease in the number of cross-bridges (Fig. 4 *D*). In cells expressing Rac1V12, we found an increased frequency of TJ strands (Figs. 4, *B* and *B′*, and Fig. 5). Significantly, as in the case of RhoAV14 cells, TJ strands in Rac1V12 cells were not only confined to the apical membrane, but also extended down the lateral membrane to the base of the cell (Fig. 4, *B* and *B′*).

In summary, freeze-fracture EM and functional analysis revealed two important effects of RhoA or Rac1 mutants on TJ organization. First, expression of either constitutively active RhoA or Rac1 resulted in the general disorganization of TJ strands at the apex of the lateral membrane and extension of strands down the lateral membrane to the base of cells. In contrast, expression of either dominant negative RhoA or Rac1 had little effect on strand organization or distribution relative to controls. Second, despite morphological differences in TJ strand organization in cells expressing constitutively active or dominant negative RhoA or Rac1, all RhoA and Rac1 mutants disrupted TJ gate function to ions (TER) and nonionic molecules (inulin, 3K, and 40K dextran).

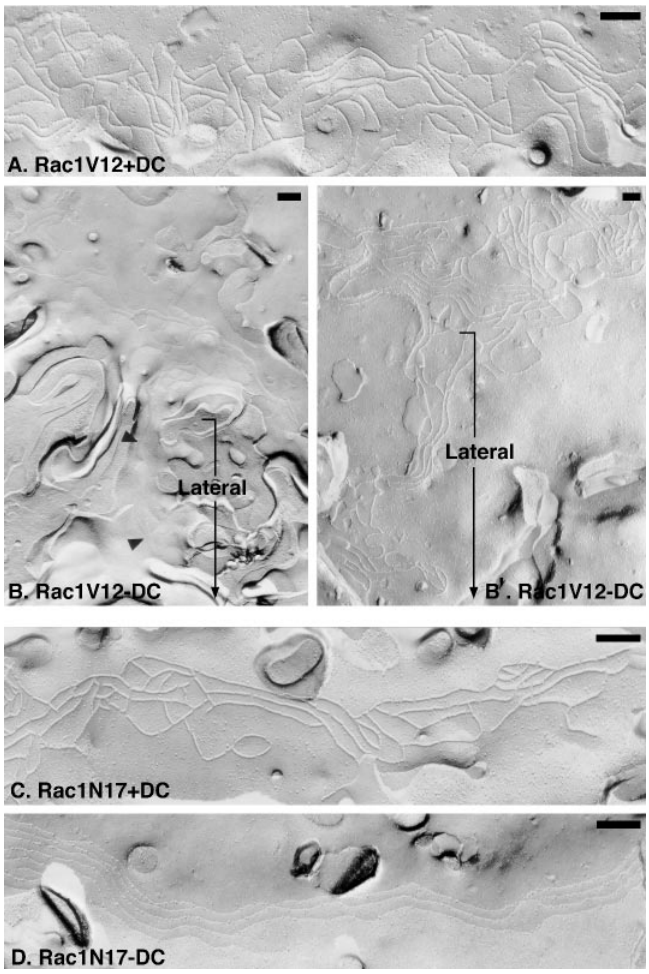

Figure 4. Freeze-fracture EM of tight junction strand organization in MDCK cells expressing Rac1 mutants. (*A*, *B*, and *B′*) Representative *P* fracture face of a TJ from Rac1V12 +DC cells (*A*) or *E* and *P* fracture face of Rac1V12-DC cells (*B* and *B′*, respectively). Fracture planes are oriented with the apical membrane at the top (from left to right) and lateral membranes oriented downwards (*bracket*). Note that strands extend from the tight junction network down the lateral membrane to the base of the cells in Rac1V12 -DC (*B* and *B′*). (*C* and *D*) Representative *P* fracture face of a TJ from Rac1N17 +DC cells (*C*) and *E* fracture face of a TJ from Rac1N17 −DC cells (*D*). There is a relative paucity of cross-bridges in the TJ network, and a few TJ strands extend basally on the lateral membrane surface in Rac1N17 −DC. Bars, 200 nm.

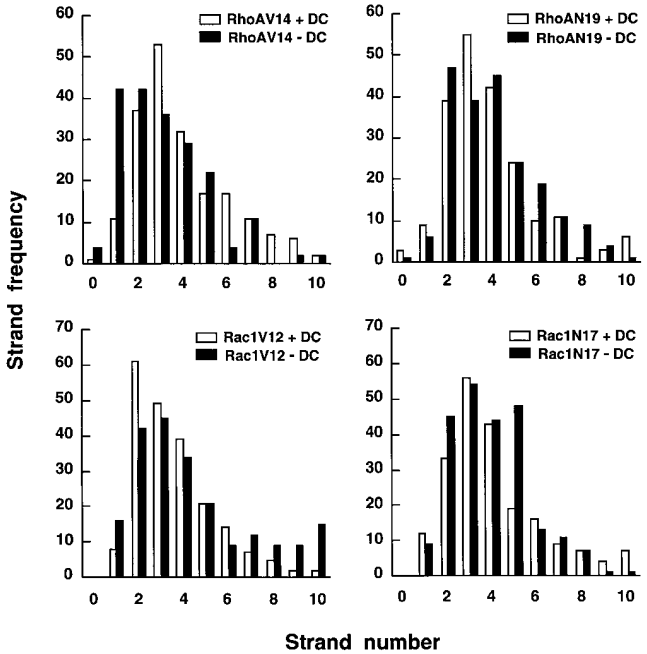

Figure 5. Quantitative analysis of TJ strand counts from freeze-fracture replicas of cells expressing RhoAV14, RhoAN19, Rac1V12, or Rac1N17 (−DC) and their matched controls (+DC); see Materials and Methods for details.

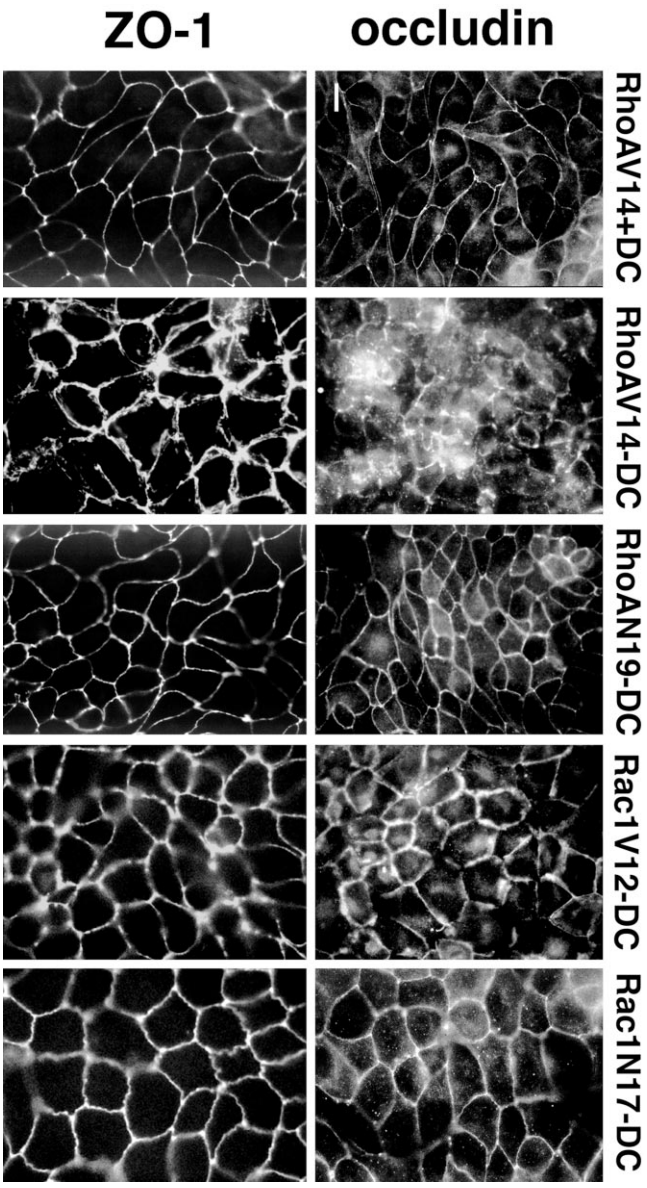

Figure 6. Indirect immunofluorescence microscopy of occludin and ZO-1 in MDCK cells expressing RhoA and Rac1 mutants. MDCK cells expressing RhoAV14, RhoAN19, Rac1V12, or Rac1N17 were grown in the presence (control, + 20 ng/ml DC) or absence of DC (−DC) for 36 h at a confluent cell density on collagen-coated glass coverslips. Cells were processed for immunofluorescence with either occludin or ZO-1 antibodies, as described in detail in Materials and Methods. Stained cells were viewed with a Axioplan microscope (Carl Zeiss, Inc.) equipped for epifluorescence. Bar, 10 μm.

Disruption of Occludin and ZO-1 Distributions by Constitutively Active, but not by Dominant Negative RhoA and Rac1 Mutants

We examined whether changes in TJ gate function and strand organization induced by RhoA and Rac1 mutants correlated with changes in the organization of occludin, a TJ transmembrane protein (Furuse et al., 1993), and ZO-1, a TJ plaque protein (Itoh et al., 1993; Willott et al. 1993; Jesaitis and Goodenough, 1994). Immunofluorescence microscopy of control cells (e.g., RhoAV14+DC) revealed sharp circumferential organizations of both occludin and ZO-1 at the apex of the lateral membrane between adjacent cells (Fig. 6); the distribution of these proteins was identical to those in parental T23 cells (data not shown). In RhoAV14 cells, occludin was chaotically distributed with discontinuous membrane and cytosolic staining. In some RhoAV14 cells, ZO-1 staining appeared to be separated into several overlapping lines instead of the sharp line that circumscribed the apex of control cells (Fig. 6). In contrast, occludin and ZO-1 in RhoAN19 cells exhibited normal organizations that were similar to those in control cells (Fig. 6).

In Rac1V12-expressing cells, occludin staining circumscribed the apical membrane at the apex of the lateral membranes, although lines of staining were often discontinuous at the vertices of contacts between three or more cells (Fig. 6). Occludin staining was also thicker en face than in control cells (Fig. 6), and appeared more like the lateral membrane staining of E-cadherin (data not shown). ZO-1 staining in Rac1V12 cells was not as sharp, but was more thick than in control cells, and the lines of ZO-1 appeared beaded rather than continuous (Fig. 6). In contrast, the staining patterns of occludin and ZO-1 in Rac1N17 cells appeared similar to those in control cells (Fig. 6).

TJ protein distributions were examined further by laser scanning confocal microscopy (Fig. 7). In control cells (e.g., RhoAV14+DC), both occludin and ZO-1 were restricted to the top of the lateral membrane at the junction with the apical membrane, and little or no staining was detected on apical, lateral, or basal membranes (Fig. 7). However, in RhoAV14- or Rac1V12-expressing cells, both occludin and ZO-1 distributions were disorganized; staining was not confined to the apex of lateral membrane, but was present along the whole length of the lateral membrane (Fig. 7). Furthermore, linear arrays of occludin and ZO-1 staining were frequently interrupted and, in some areas, separated into several parallel or interwoven strands (Fig. 7). In general, occludin and ZO-1 staining appeared more disorganized in cells expressing RhoAV14. Occludin and ZO-1 distributions in RhoAN19- or Rac1N17-expressing cells appeared normal and similar to those in control cells (Fig. 7).

We conclude that normal patterns of occludin and ZO-1 staining in control cells and Rac1N17- and RhoAN19-expressing cells correlated well with normal TJ strand organization observed by freeze-fracture EM. Abnormalities in occludin and ZO-1 organization (discontinuities, separated lines, and lateral membrane distribution) in cells expressing RhoAV14 and Rac1V12 correlated with disorganized, interwoven and lateral membrane strands observed by freeze-fracture analysis.

Reversibility of TJ Structural and Functional Defects Induced by RhoA and Rac1 Mutants

A DC switch protocol was used to test whether the effects of RhoA and Rac1 mutants on TJ structure and function were reversible (Fig. 8). Two cultures were initiated for each cell line; one culture formed cell–cell contacts in the presence of DC (i.e., in the absence of mutant protein expression), and the other formed cell–cell contacts in the

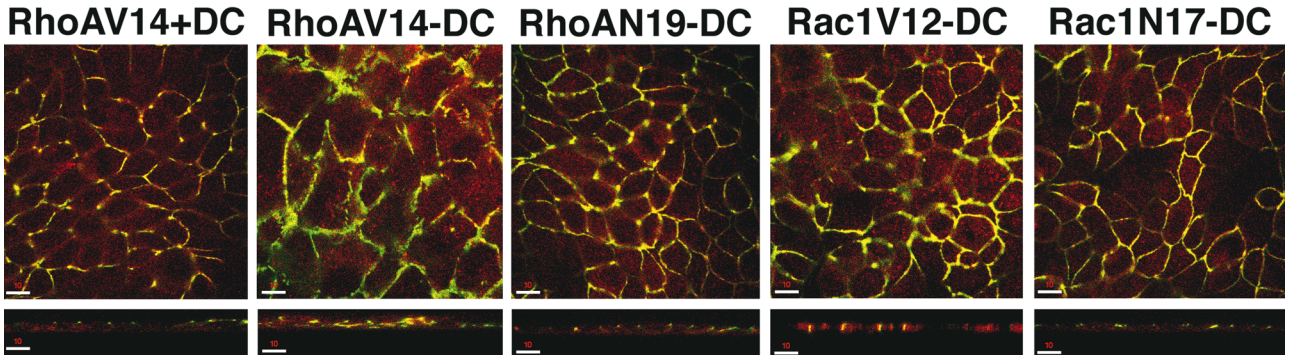

Figure 7. Confocal microscopy analysis of occludin and ZO-1 distribution in MDCK cells expressing RhoA and Rac1 mutants. MDCK cells expressing RhoAV14, RhoAN19, Rac1V12, or Rac1N17 were grown in the presence (control, + 20ng/ml DC) or absence of DC (−DC) for 36 h at a confluent cell density on collagen I–coated glass coverslips. Cells were fixed, permeabilized, and double-stained with rabbit antioccludin antibody and rat anti-ZO-1 R40.76 hybridoma supernatant, followed by rhodamine-conjugated goat anti–rabbit and FITC-conjugated goat anti–rat secondary antibodies. The images were collected with a laser scanning confocal microscope Multi-Probe 2010™ (Molecular Dynamics, Inc.). Bar, 10 μm.

absence of DC (i.e., mutant proteins were expressed). After 32 h, TJs in control cells (T23, pUHD ± DC) or cells in which mutant RhoA or Rac1 expression had been repressed (+DC) had established TER of 200–300 ohms per cm^2. In contrast, cells expressing RhoA or Rac1 mutants (−DC) generally had considerably lower TER values than did control cells (Fig. 8), as expected (see also Fig. 1).

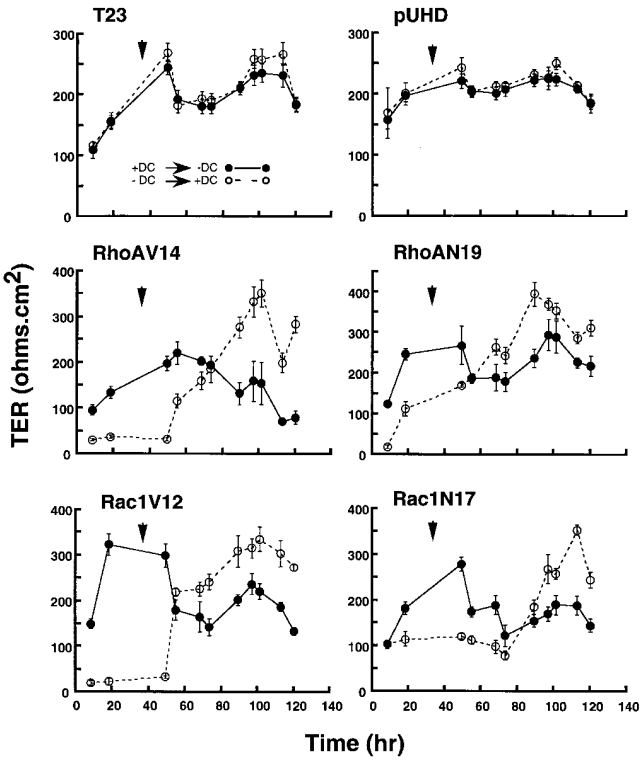

Figure 8. DC switch experiment to examine the reversibility of defects in TJ function caused by RhoA and Rac1 mutants. MDCK cells expressing RhoAV14, RhoAN19, Rac1V12, or Rac1N17 were divided into two populations. One population of each cell line (+DC →−DC group) was grown initially in DMEM/FBS + 20 ng/ml DC, and then switched to medium without DC at the indicated time (*arrowhead*). The other population (−DC → +DC group) was grown at first without DC and then switched to medium containing 20 ng/ml DC (*arrowhead*). 2.5 mM sodium butyrate was added between 56 and 96 h to enhance RhoA and Rac1 mutant expression. TER was measured in quadruplicate cultures, and is reported as mean ± SEM.

DC was removed from the +DC control cells (+DC → −DC group) to allow Rac1 or RhoA mutant expression, and was added to cells to repress RhoA or Rac1 mutant expression (−DC → +DC group); the time of the DC switch is marked by an arrowhead in Fig. 8. In addition, 2.5 mM Na-butyrate was added to the culture medium between 56 and 92 h to induce RhoA or Rac1 mutant expression further in the +DC → −DC group; Na-butyrate decreased TER in control cells by <20%, but had no effect on recovery of TER in the −DC → +DC group (Fig. 8). After a delay, the TER of the +DC → −DC group began to decrease; the final TER level obtained at 120 h was similar to the TER at the beginning of TJ assembly when RhoA or Rac1 mutants were not expressed, but was generally higher than the TER of the same cells when RhoA or Rac1 mutants were expressed throughout the period of TJ formation. Those cell lines that had formed a leaky monolayer (TER, ~15–120 ohms per cm^2) during the period when RhoA or Rac1 mutants were expressed (−DC), were converted to a tighter monolayer (TER, >300 ohms per cm^2) upon repression of RhoA or Rac1 mutant expression (+DC); the kinetics of TER development were similar in this group to those in control cells during TJ formation in the absence of RhoA or Rac1 mutant expression (Fig. 8). In general, the final TER level obtained after 120 h was similar to the maximum levels obtained when TER developed in the absence of RhoA or Rac1 mutant expression.

For comparison with TJ function, the distributions of occludin and ZO-1 were examined by immunofluorescence microscopy at the end of the DC switch protocol; myc antibody staining was used to monitor the expression or repression of RhoA or Rac1 mutants in the +DC → −DC and −DC → +DC groups, respectively (Fig. 9). Little or no myc staining was detected in all the −DC → +DC group cells, demonstrating that RhoA or Rac1 mutant expression had been repressed. In the −DC → +DC group of cells, occludin and ZO-1 staining sharply circumscribed each cell at the apex of lateral membranes (Fig. 9), similar to staining patterns of these proteins in control cells (see

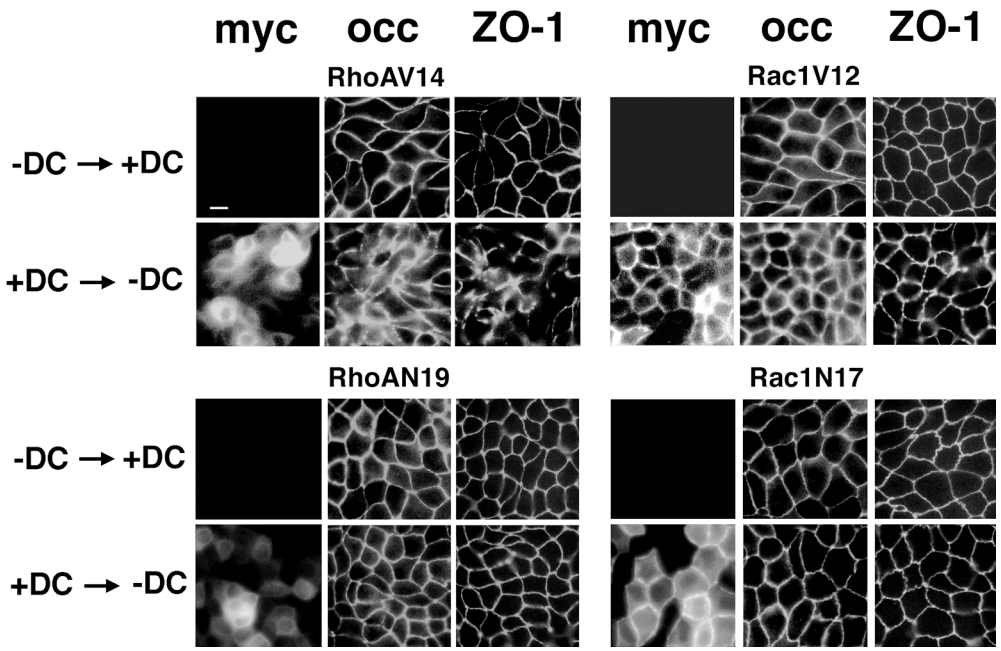

Figure 9. Indirect immunofluorescence of myc-tagged RhoA or Rac1 mutants, occludin, and ZO-1 distributions at the end of the DC switch experiment shown in Fig. 8. MDCK cells expressing RhoAV14, RhoAN19, Rac1V12, or Rac1N17 were divided into two populations. One population of each cell line was grown initially in DMEM/FBS + 20 ng/ml DC, and then switched to medium without DC 32 h later (+DC → −DC group). The other population (−DC → +DC group) was grown at first without DC and then switched to medium containing 20 ng/ml DC. 2.5 mM sodium butyrate was added between 56 and 96 h to enhance RhoA and Rac1 mutant expression. Immunofluorescence was performed at the end of the DC switch experiment by staining the filters with mouse anti-myc antibody (to identify the myc-tagged RhoA or Rac1 mutant), rabbit anti-occludin antibody, and rat anti-ZO-1 (R40.76 hybridoma) antibody. Cells were examined in a Axioplan™ microscope (Carl Zeiss, Inc.) equipped with epifluorescence. Bar, 10 μm.

Fig. 6). The normal distributions of occludin and ZO-1 correlated with the recovery of high TER values in those cells (see Fig. 8).

In the +DC → −DC group, myc staining showed that RhoAV14 and Rac1V12 were expressed and distributed in the cytoplasm and cell–cell contacts, respectively, as expected (see Fig. 3 in Jou and Nelson, 1998). RhoAV14 and Rac1V12 expression correlated with abnormal occludin and ZO-1 distributions (Fig. 9), as expected (see Figs. 6 and 7). RhoAN19 and Rac1N17 were localized to the cytoplasm and cell–cell contacts, respectively (Fig. 9), as expected (Fig. 3 in Jou and Nelson, 1998). Occludin and ZO-1 staining in RhoAN19 and Rac1N17 cells appeared normal, and was similar to that in control cells (Figs. 6 and 7) even though these cells had functionally leaky TJ (Fig. 8).

The reversibility of the effects of RhoA and Rac1 mutants on both TJ function and protein distributions shows that Rac1 and RhoA regulate TJ function transiently, and not in a toxic fashion. Furthermore, both TJ structure and function are dynamic and subject to RhoA and Rac1 regulation, even after the junctional complex has been fully assembled and tightly sealed.

TJ Fence Function is Perturbed by RhoA and Rac1 Mutants

In addition to forming a gate to paracellular flow, the TJ also forms a fence for free diffusion of lipids in the outer leaflet of the plasma membrane between the apical and basal-lateral membrane domains. We compared TJ fence function in control cells and cells expressing RhoA or Rac1 mutants by analyzing lipid diffusion (Fig. 10). Apical membranes were labeled with BODIPY-sphingomyelin for 10 min on ice. The cells were then washed extensively and either immediately processed for confocal microscopy

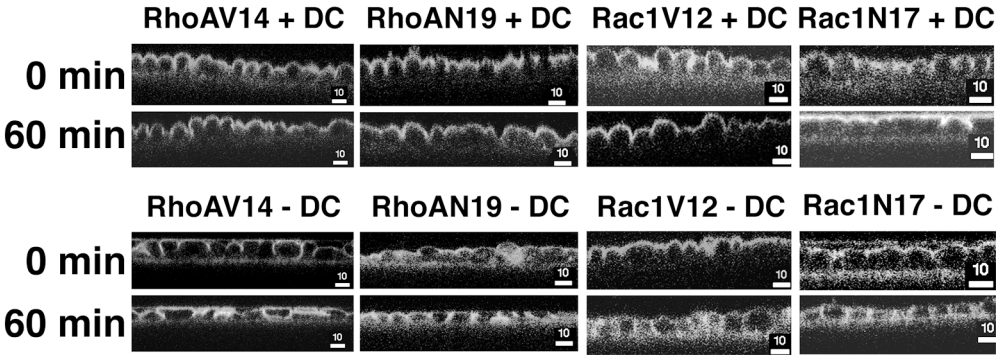

Figure 10. Diffusion of fluorescent lipid from the apical to lateral membranes in cells expressing RhoA and Rac1 mutants. MDCK cells expressing RhoAV14, RhoAN19, Rac1V12, or Rac1N17 were cultured on Transwell™ filters in the presence (+DC) or absence (−DC) of DC. The apical surface was incubated in BODIPY-sphingomyelin/BSA complex solution on ice for 10 min (see Materials and Methods). The cells were washed three times in P buffer, and were then either immediately processed for microscopy (*0 min*) or incubated for an additional 60 min (*60 min*) on ice before processing. The distribution of fluorescent lipid was determined with a Molecular Dynamics confocal microscope, and representative *xz* projections are shown. Bar, 10 μm.

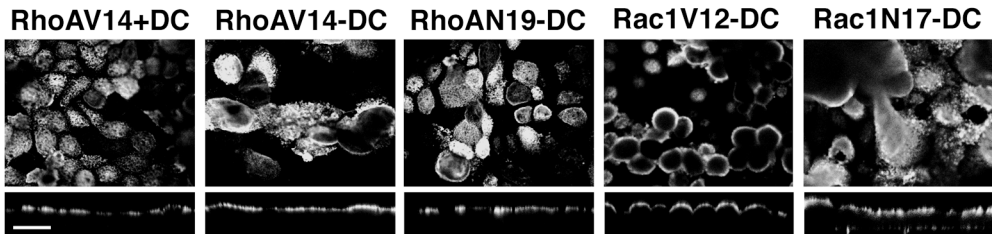

Figure 11. Distribution of the apical membrane protein, $p75^{NTR}$, in MDCK cells expressing RhoA and Rac1 mutants. MDCK cells expressing RhoAV14, RhoAN19, Rac1V12, or Rac1N17 were grown in the presence (+DC) or absence (−DC) of 20 ng/ml DC at low cell density for 20 h, trypsinized, and plated at confluent cell density on Transwell™ filters. Cells were incubated for a further 48 h in the presence or absence of 20 ng/ml DC. $p75^{NTR}$-expressing adenovirus was applied to the monolayer. 24 h after adenovirus infection, filters were fixed, permeabilized, and double-stained with mouse anti-p75 and rabbit anti-myc antibody followed by FITC-conjugated goat anti–mouse and rhodamine-conjugated goat anti–rabbit secondary antibodies. Cells were examined with a Molecular Dynamics confocal microscope, and representative stacked *xy* and *xz* projections of $p75^{NTR}$ staining are shown. Bar, 10 μm.

(0 min) or incubated in buffer for a further 60 min on ice. As shown in Fig. 10, membrane-labeled BODIPY–sphingomyelin was restricted to the apical membrane of controls cells (+DC) after either the 10-min pulse (0 min) or the 60-min chase; note that the apical membrane is domed in the *xz* profile, which can give the erroneous appearance of lateral membrane staining.

In cells expressing RhoAN19, Rac1V12, or Rac1N17, BODIPY-sphingomyelin labeled the apical membrane after the 10-min pulse (0 min), but not the lateral membrane; some lateral membrane labeling was detected in cells expressing RhoAV14, although the apical membrane was also very domed in these cells (Fig. 10). After a 60-min chase, BODIPY-sphingomyelin was detected in both the apical and lateral membranes of all cells expressing RhoA or Rac1 mutants (Fig. 10).

The gate function of TJs in RhoA- and Rac1-expressing cells is disrupted (Figs. 1 and 2). Therefore, it is possible that lateral membrane labeling with BODIPY-sphingomyelin in these cells was the result of lipid diffusing in solution across the TJ. To test for this possibility, an aliquot of solution was recovered from the apical and the basal compartment of each filter after the 10-min pulse. Spectroscopic measurement of BODIPY-sphingomyelin levels showed that <0.1% of the fluorescence present in the apical compartment had leaked into the basal compartment during the labeling period (data not shown), indicating that lateral membrane labeling with BODIPY-sphingomyelin was most likely due to diffusion of lipid in the plane of the lipid bilayer. In addition, we included BSA in the chase P buffer in order to exclude the possibility that the presence of BODIPY-sphingomyelin in the lateral membranes of these cells was due to exchange of apical membrane BODIPY-sphingomyelin into the buffer, and then reinsertion into the lateral membrane. Although the fluorescence signal was diminished in all membranes due to direct extraction of some lipid by BSA, we still detected BODIPY-sphingomyelin in the lateral membranes of cells expressing mutant RhoA or Rac1 (data not shown).

Effects of Mutant RhoA and Rac1 on Protein Delivery to the Apical Membrane

As the TJ fence-to-lipid diffusion is disrupted in cells expressing RhoA or Rac1 mutants, we considered whether the organization of membrane proteins at apical and basal-lateral membrane domains was also disrupted. We examined delivery to the cell surface and membrane domain organization of $p75^{NTR}$ (Fig. 11), a membrane protein that is targeted and restricted to the apical membrane of MDCK cells (Le Bivic et al., 1991; Yeaman et al., 1997). MDCK cells were grown at low density for 24 h without DC to induce expression of RhoA or Rac1 mutants. Cells were trypsinized and plated at confluent density in LCM, and then switched to HCM to induce cell–cell adhesion for 24 h. Cells were infected with recombinant adenovirus encoding $p75^{NTR}$, and then processed for immunofluorescence after a further 24 h. Results show clearly that $p75^{NTR}$ was localized to the apical membrane of cells expressing either RhoAV14, RhoAN19, Rac1V12, or Rac1N17; little or no staining was detected on lateral or basal membranes (Fig. 11). These results indicate that delivery of $p75^{NTR}$ from the TGN to the apical membrane was not disrupted in the presence of RhoA or Rac1 mutants, and that $p75^{NTR}$ did not diffuse from the apical membrane across the TJ into the lateral membrane.

Expression of Mutant RhoA or Rac1 Does Not Change the Expression of the Occludin/ZO-1/ZO-2 Complex, but Affects the Detergent Solubility of ZO-1

Effects of mutant RhoA and Rac1 expression on steady-

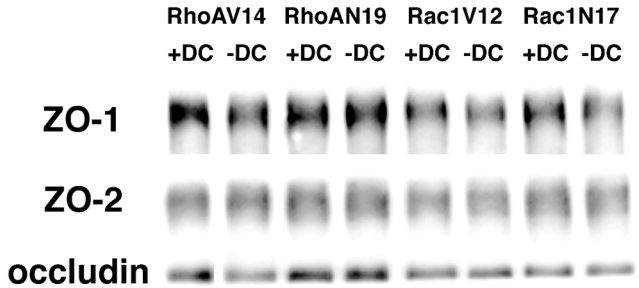

Figure 12. Western blot analysis of occludin, ZO-1, and ZO-2 levels in MDCK cells expressing RhoA and Rac1 mutants. 30 μg of total protein lysates from MDCK cells expressing RhoAV14, RhoAN19, Rac1V12, or Rac1N17 grown in the presence (+DC) or absence (−DC) of 20 ng/ml DC was separated by SDS-PAGE, proteins were transferred electrophoretically to nitrocellulose filters and probed with antibodies specific for ZO-1, ZO-2, and occludin. For details, see Materials and Methods.

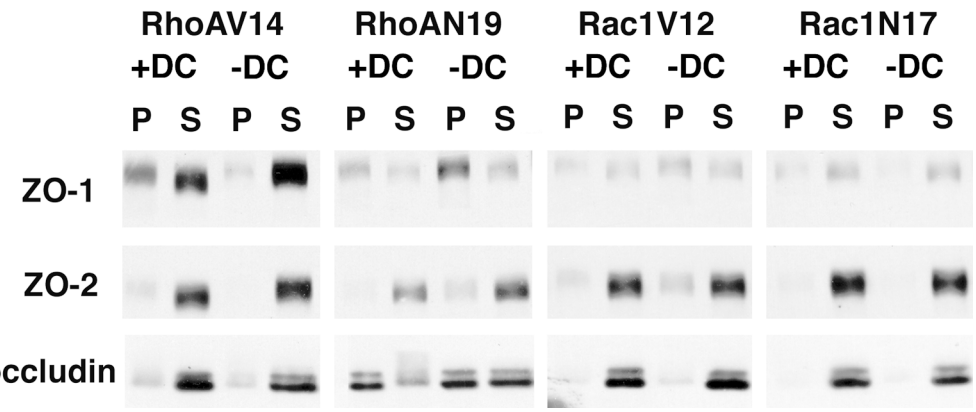

Figure 13. Triton X-100 solubility of occludin, ZO-1, and ZO-2 in MDCK cells expressing RhoA or Rac1 mutants. MDCK cells expressing RhoAV14, RhoAN19, Rac1V12, or Rac1N17 were grown in the presence (+DC) or absence (-DC) of 20 ng/ml DC on Transwell™ filters. Cells were extracted in buffer containing 1% Triton X-100 on ice for 20 min, and equal portions of the pellet (*P*) and supernatant (*S*) were separated by high-speed centrifugation. Proteins in equal amounts of pellet and supernatant samples were separated by SDS-PAGE, transferred electrophoretically to nitrocellulose filters, and probed with antibodies specific for ZO-1, ZO-2, and occludin. For details, see Materials and Methods.

state protein levels of occludin, ZO-, and ZO-2 were examined in Western blots of whole-cell lysates. In general, steady-state levels of occludin, ZO-1, and ZO-2 were similar in cells expressing RhoAN19, Rac1V12, or Rac1N17, and control cells (+DC; Fig. 12). Expression of RhoAV14 coincided with a small decrease (25% decrease compared with the protein level in control cells) in the level of occludin, but there was little or no change in levels of either ZO-1 or ZO-2.

We sought to examine whether mutant RhoA or Rac1 affected the occludin/ZO-1 complex. We attempted to coimmunoprecipitate the complex with occludin antibodies and blot back with ZO-1 antibodies. We detected ZO-1 in occludin-specific immunoprecipitates from both control cells and cells expressing RhoA or Rac1 mutants, but the ZO-1 signal was too low in both cases to draw any strong conclusion (data not shown). We also used Superose 6 FPLC to fractionate proteins from detergent extracts of cells expressing RhoA or Rac1 mutants. Results showed little or no association of these proteins under these extraction and separation conditions; we did not detect any change in the elution profiles of occludin, ZO-1, or ZO-2 compared with the appropriate controls (data not shown).

Finally, we examined whether there were any differences in the extractability of the occludin/ZO-1/ZO-2 complex from cells in buffer containing Triton X-100 (Fig. 13). In control cells, most of the ZO-1, ZO-2, and occludin were extracted from cells. However, in cells expressing RhoAV14, we detected an increase in the Triton X-100 solubility of ZO-1. In contrast, expression of dominant negative RhoA coincided with a decrease in ZO-1 extractability. We did not detect any change in the Triton X-100 extractability of occludin or ZO-2 in cells expressing either constitutively active or dominant negative RhoA or Rac1 mutants.

Discussion

Previous studies of RhoA family members have mostly focused on the effects of mutant RhoA or Rac1 on actin, and the consequential changes in actin structures at the plasma membrane of single, motile cells (Hall, 1998). The role(s) of RhoA and Rac1 in regulating other cellular structures, particularly in the context of the organization of epithelial cells in tissues, is less well understood. Here, we focused on the effects of mutant RhoA or Rac1 expression on TJ gate and fence functions. Our results indicate that RhoA and Rac1 regulate both the gate and fence functions of the TJ, and effect restriction of TJ proteins to the boundary of the apical/lateral membranes.

TJ Gate and Fence Functions are Disrupted by RhoA and Rac1 Mutants

TJ gate function was assessed by measuring the TER and nonionic molecules (inulin, 3K, and 40K dextran) through the paracellular pathway. We found that gate function was very sensitive to disruption by levels of expression of either constitutively active or dominant negative RhoA or Rac1 that were 10–40% of the levels of endogenous RhoA or Rac1. That substoichiometric levels of RhoA or Rac1 mutants disrupted TJ function indicates that mutant GTPases displace rapidly cycling endogenous GTPases from targets and, because catalytic cycling is inhibited by the mutation, mutant proteins remain bound to the target and accumulate, thereby resulting in quick domination of the mutant phenotype (see also Jou and Nelson, 1998).

In addition to disrupting gate function, we showed that RhoA and Rac1 mutants disrupted TJ fence function as indicated by the diffusion of BODIPY-sphingomyelin from the apical to the lateral membrane. That sphingomyelin was apparently free to diffuse across the TJ was surprising in light of the results of the preceding study in which E-cadherin was correctly localized to the basal-lateral membrane in the same cells (Jou and Nelson, 1998). However, the distribution of E-cadherin may not be a good test of TJ fence function as E-cadherin binds to the actin cytoskeleton (Nagafuchi and Takeichi, 1988), which restricts its mobility in the plane of the lipid bilayer (C. Adams, Y.-T. Chen, S. J. Smith, and W.J. Nelson, manuscript submitted for publication). The apical membrane protein $p75^{NTR}$ is a better test since it does not bind to the actin cytoskeleton (Le Bivic et al., 1991; Yeaman et al., 1997). Using an adenovirus-mediated expression system to pulse-express $p75^{NTR}$, we found that $p75^{NTR}$ accumulated

in the apical membrane of control cells and cells expressing RhoA or Rac1 mutants. These results show that the TJ fence-to-protein diffusion was not disrupted, and indicate that TJ protein/strand organization is sufficiently disrupted to allow lipids, but not proteins, to diffuse through the TJ fence.

Significantly, we found that disruptions of TJ gate and fence functions by RhoA and Rac1 mutants did not correlate with a direct role of RhoA or Rac1 in regulating TJ protein organization. Although RhoAV14 and Rac1V12 disrupted TJ function and protein and strand organization, neither RhoAN19 nor Rac1N17 caused gross changes in occludin or ZO-1 distributions or TJ strand organization. Dominant negative mutant GTPases are thought to affect endogenous GTPase functions by sequestering regulators of the GTPase cycle (e.g., GEF), thereby inhibiting the activity of the endogenous GTPase (Boguski and McCormick, 1993); in this capacity, the expression level of a dominant negative mutant is likely to be critical. We note that effects on TER were detected at levels of expression of RhoAN19 and Rac1N17 that were 13 and 50% of endogenous RhoA and Rac1 levels, respectively (Jou and Nelson, 1998), indicating that changes in TJ organization were acutely sensitive to levels of dominant negative RhoA and Rac1. In addition, while full expression of RhoAN19 was only 60% of the endogenous RhoA level, Rac1N17 was expressed at >600% of the level of endogenous Rac1 (Jou and Nelson, 1998). Together, these results indicate that expression levels of RhoAN19 and Rac1N17 were sufficiently high to affect TJ function, but not TJ protein organization.

The effects of RhoA mutants on TJ structure and function that we observed are different from those reported in previous studies. Nusrat et al. (1995) used a recombinant bacterial toxin to deliver C3, an inhibitor of endogenous RhoA function, into T84 cells. They observed a defective TJ gate function and loss of ZO-1 staining from the TJ region. Our results show that dominant negative RhoA (RhoAN19) expression induced a leaky TJ gate junction in MDCK cells without any apparent effects on either TJ protein (occludin, ZO-1) localization or TJ strand organization. The discrepancy between these results could be due to the different expression systems adopted, or the level of expression of either C3 toxin or mutant protein (but see above). We note, however, that a morphologically normal but functionally defective TJ has been described in animal models of colitis in which intestinal and biliary epithelia became leaky without any accompanying morphological changes to the TJ (Cui et al., 1996; Lora et al., 1997).

During final stages of the present work, Takaishi et al. (1997) reported the effects of constitutively expressed RhoA and Rac1 mutants on MDCK cells. They observed no effect of RhoAV14, Rac1V12, or Rac1N17 expression on ZO-1 distribution compared with an untransfected control cell population. Effects of RhoAN19 on cells were not presented. However, microinjection of C3 exoenzyme disrupted the distribution of ZO-1 in some cells, but not in others. In comparison to our results, it is unclear why Takaishi et al. (1997) did not detect morphological changes to the TJ in MDCK cells expressing either RhoAV14 or Rac1V12. A possible explanation is that different amounts of RhoA and Rac1 mutants were expressed. Takaishi et al. (1997) reported that the amount of RhoAV14 was <10% of that of endogenous RhoA, and Rac1V12 and Rac1N17 expression could not be detected in Western blots of whole cell extracts.

Roles of RhoA and Rac1 in Regulating TJ Assembly, Structure, and Function

Based on our direct comparison of TJ function with TJ structure, we can identify at least two levels of TJ regulation by RhoA and Rac1. One level involves an indirect effect on mechanisms involved in restricting TJ proteins and strands to the boundary of the apical/lateral membrane. The second level involves direct regulation of TJ gate, and at least some fence functions. Regulation of TJ structure and function by RhoA and Rac1 is likely to be very dynamic. The DC switch experiment (Figs. 8 and 9) showed that effects of these mutants on TJ structure and function were completely reversible, and that expression of each mutant could disrupt TJs that had formed normally. That both active and dominant negative forms of RhoA or Rac1 have similar effects on TJ structure and function is not unexpected, as both mutant forms of GTPases have been shown to have similar rather than opposite effects in other cell culture systems (Stowers et al., 1995; Anand et al., 1997) or whole organisms (Luo et al., 1994).

Role of RhoA and Rac1 in TJ Assembly

Although all cells expressing RhoA and Rac1 mutants exhibited disrupted gate and fence functions, only cells expressing constitutively active RhoA (RhoAV14) and Rac1 (Rac1V12) had clearly disrupted TJ structures. TJ strands and occludin/ZO-1 staining circumscribed the apical membrane, but the organization was chaotic as parallel strands/rings of protein separated over a short distance and then interwove with each other. Most striking, however, was the finding that TJ strands and occludin/ZO-1 staining extended down the whole length of the lateral membrane to the base of cells expressing RhoAV14 or Rac1V12. The structural basis for this gross disruption of TJ structure is not known. We did not detect major changes in the steady state amounts of occludin, ZO-1, or ZO-2, except a 25% decrease in occludin levels in RhoAV14-expressing cells. We attempted several approaches to identify an occludin/ZO-1 complex, but even in control cells the complex was easily disrupted during protein extraction. However, we detected a small but reproducible increase in the Triton X-100 extractability of ZO-1 in RhoAV14 mutant–expressing cells, but not occludin or ZO-2, that might reflect a change in the binding of ZO-1 to actin filaments or a change in actin organization. We note that these gross defects in TJ strand organization and protein distributions in the presence of Rac1V12 and RhoAV14 were completely and rapidly reversed upon repression of mutant gene expression (DC switch experiment, see Fig. 8), indicating that they were neither toxic nor a dead end in the assembly of a functional TJ.

Previous studies have shown that TJ assembly is dependent on cadherin-mediated cell–cell adhesion (Gumbiner et al., 1988). Furthermore, the distributions of occludin/

ZO-1 and cadherin are initially similar upon cell–cell adhesion, but subsequently occludin/ZO-1 dissociates from the cadherin organization and redistributes to the apex of the lateral membrane together with the cortical actin belt (see van Itallie and Anderson, 1997). We suggest that the abnormal organization of occludin/ZO-1 at the lateral membrane of polarized cells expressing Rac1V12 or RhoAV14 is due to an inhibition of this latter step in TJ assembly. Although the mechanisms involved are not known, we speculate that changes to the normal organization of the actin cytoskeleton at cell–cell contacts may inhibit dynamic alterations in occludin/ZO-1 distribution necessary for TJ assembly. We found that expression of RhoAV14 and Rac1V12 caused dramatic changes in actin organization, including clumping at the apical membrane (Rac1V12), formation of thick bundles at the lateral membrane (Rac1V12), and increased numbers of stress fibers at the base of the cell (RhoAV14; Jou and Nelson, 1998). These changes in actin organization could decrease dynamic changes in protein–protein interactions that may be necessary to separate occludin/ZO-1 complexes from E-cadherin/catenin complexes to assemble the TJ at the apex of the lateral membrane.

In the context of the lateral membrane distribution of occludin in Rac1V12 and RhoAV14 cells, it is striking that a similar lateral membrane distribution has been described in proximal convoluted renal tubules of human (Kwan, O., G.D. Myers, R. Sibley, D. Dafoe, E. Alfrey, and W.J. Nelson, manuscript submitted for publication) and mouse (P. Piepenhagen and W.J.Nelson, unpublished results); in distal convoluted tubules, occludin staining is restricted to the apex of the lateral membrane (O. Kwan, G.D. Myers, R. Sibley, D. Datoe, E. Alfrey, and W.J. Nelson, manuscript submitted for publication). Significantly, proximal renal tubule epithelia are classified as leaky, whereas distal tubule epithelia are classified as tight. We do not know if occludin distribution is regulated by RhoA family members in renal tubule epithelia, but Rho-related small GTP-binding proteins are enriched in regions of kidney cortex that contain proximal convoluted tubules (Boivin and Beliveau, 1995).

Roles of RhoA and Rac1 in TJ Structure and Function

The structural basis for TJ gate and fence functions is poorly understood. Previous studies sought to establish a relationship between TJ strand number and function (Claude, 1978), but it has been difficult to extrapolate generalizations to all cell types (Stevenson et al., 1988). Our studies showed that TJ strand organization in RhoAN19 and Rac1N17 cells appeared normal, but TJ fence and gate functions were disrupted. In the case of the TJ fence we found that the barrier to lipid, but not protein diffusion, was disrupted. It is possible that maintenance of TJ fence function to protein diffusion in these mutants might not be due to the TJ fence per se, but to a general decrease in protein mobility as a result of global changes in the actin cytoskeleton and actin-associated membrane proteins (see Jou and Nelson, 1998). Alternatively, there might be sufficient structural organization in the TJ to prevent protein, but not lipid diffusion, into the lateral membrane in cells expressing RhoA/Rac1 mutants. In this latter case, the TJ fence would behave as a molecular sieve that determines molecule diffusion based on size; size selectivity could be modulated by adjusting the number of parallel strands, the spacing between parallel strands, and the frequency of cross-bridges. A similar mechanism could regulate TJ gate function, in which interdigitating TJ strands on the extracellular surface of opposing membranes form a molecular sieve to regulate ion and solute diffusion along the paracellular pathway.

At present it is not clear how TJ protein organization might alter TJ barrier functions. Although recent studies have cast doubt on the central role of occludin in TJ functions (Saitou et al., 1998), earlier studies indicated that changes in the amount of occludin expressed and its protein interactions might be functionally important. For example, overexpression of COOH-terminal truncated occludin caused a two to threefold increase in TER and an increase in tracer diffusion through the paracellular space, but normal TJ strand organization (Balda et al., 1996). Overexpression of full- length occludin in MDCK cells also resulted in an ~35% increase in TER and an increase in tracer diffusion across the monolayer, but an increase in TJ strand number and network width (McCarthy et al., 1996). At present, it is not clear whether changes in RhoA/Rac1 functions and altered TJ structure by overexpressing occludin disrupt TJ function through the same or different pathways.

How might RhoA or Rac1 regulate the organization of TJ strands/protein complexes to specify gate and fence functions? We did not find gross abnormalities in TJ strand/protein organization in the presence of dominant negative RhoA or Rac1, indicating that neither RhoA nor Rac1 activity is necessary at this level of organization. Alternatively, RhoA and Rac1 could regulate TJ gate and fence functions via the actin cytoskeleton by altering the forces that push cells together and/or the complexity of strand organization. Madara (Madara et al., 1988) suggested that TJ functions could be modified by contraction of perijunctional actin filaments that could result in centrifugal traction on TJ membrane contacts. Changes in actin contractility could subtly alter the distance between parallel strands and/or between cross-bridges to modulate fence function, and regulating centrifugal traction could change the force pushing strands together on opposing cell surfaces to modulate gate function. The actin cytoskeleton is a target for RhoA and Rac1 activities (Hall, 1998). It is possible that rapid cycling (flickering) of RhoA and Rac1 GTPases between GTP- and GDP-bound forms is required to fine-tune tension in the cortical actin belt, and thereby modulate TJ structure to a specific gate and fence function. That the permeability of epithelia can be converted from tight to leaky under physiological conditions (Madara, 1988; Madara, et al., 1986) and by expressing RhoA or Rac1 mutants (this study) supports the view that mechanisms involved in regulating TJ functions are dynamic.

The targets of RhoA and Rac1 that regulate TJ functions will need to be identified. Although several targets have identified in single motile cells, they too may be candidates for regulating TJ functions in epithelia. These candidates include downstream targets of Rho-kinase such as myosin phosphatase and the regulatory myosin light chain

(Amano et al., 1996; Kimura et al., 1996), which control the interaction of myosin with actin filaments and subsequent force generation, the ERM family of proteins (Matsui et al., 1998), and phosphatidylinositol (4,5)-bisphosphate (PIP_2) synthesis (Chong, et al., 1994) since PIP_2 has broad effects on the actin cytoskeleton (Janmey, 1994). Whether RhoA and Rac1 have the same targets is also unknown, although results reported in the accompanying study indicate that Rac1 does not function through RhoA in these cells (Jou and Nelson, 1998). The availability of stable cell lines expressing RhoA and Rac1 mutant GTPases should facilitate the identification of potential targets.

We are very grateful to the following colleagues who made various reagents available to us: Dr. Rong-Guo Qiu (Onyx Pharmaceuticals, Richmond, CA) for the RhoA and Rac1 mutant plasmids; Dr. Gordon Cann (Stanford University, Stanford, CA) for the mouse anti-myc hybridoma, 9E10; Dr. Inke Nathke (Stanford University, Stanford, CA) for the rabbit anti-β-catenin polyclonal antibody; and Dr. Charles Yeaman (Stanford University, Stanford, CA) for the mouse anti-$p75^{NTR}$ antibody and help with the adenoviral expression system. We thank members of the Nelson laboratory and Marc Symons (Onyx Pharmaceuticals, Richmond, CA) for their criticisms and help during the course of this work.

This work was supported by a grant from the National Institutes of Health to W.J. Nelson.

Received for publication 16 March 1998 and in revised form 27 May 1998.

References

Aktories, K., U. Braun, S. Rosener, I. Just, and A. Hall. 1989. The rho gene product expressed in *E. coli* is a substrate of botulinum ADP-ribosyltransferase C3. *Biochem. Biophys. Res. Commun.* 158:209–213.

Almers, W., and C. Stirling. 1984. Distribution of transport proteins over animal cell membranes. *J. Membr. Biol.* 77:169–186.

Amano, M., M. Ito, K. Kimura, Y. Fukata, K. Chihara, T. Nakano, Y. Matsuura, and K. Kaibuchi. 1996. Phosphorylation and activation of myosin by Rho-associated kinase (Rho-kinase). *J. Biol. Chem.* 271:20246–20249.

Anand, A.B., B.R. Zetter, A. Viswanathan, R.G. Qiu, J. Chen, R. Ruggieri, and M. Symons. 1997. Platelet-derived growth factor and fibronectin-stimulated migration are differentially regulated by the Rac and extracellular signal-regulated kinase pathways. *J. Biol. Chem.* 272:30688–30692.

Anderson, J.M., and C.M. Van Itallie. 1995. Tight junctions and the molecular basis for regulation of paracellular permeability. *Am. J. Physiol.* 269:G467–G475.

Balda, M.S., J.A. Whitney, C. Flores, S. Gonzalez, M. Cereijido, and K. Matter. 1996. Functional dissociation of paracellular permeability and transepithelial electrical resistance and disruption of the apical-basolateral intramembrane diffusion barrier by expression of a mutant tight junction membrane protein. *J. Cell Biol.* 134:1031–1049.

Boguski, M.S., and F. McCormick. 1993. Proteins regulating Ras and its relatives. *Nature.* 366:643–654.

Boivin, D., and R. Beliveau. 1995. Subcellular distribution and membrane association of Rho-related small GTP-binding proteins in kidney cortex. *Am. J. Physiol.* 269:F180–F189.

Cereijido, M., M.L. Gonzalez, R.G. Contreras, J.M. Gallardo, V.R. Garcia, and J. Valdes. 1993. The making of a tight junction. *J. Cell Sci. Suppl.* 17:127–132.

Chong, L.D., K.A. Traynor, G.M. Bokoch, and M.A. Schwartz. 1994. The small GTP-binding protein Rho regulates a phosphatidylinositol 4-phosphate 5-kinase in mammalian cells. *Cell.* 79:507–513.

Claude, P. 1978. Morphological factors influencing transepithelial permeability: a model for the resistance of the zonula occludens. *J. Membr. Biol.* 39:219–232.

Cui, N., K.L. Madsen, D.R. Friend, B.R. Stevenson, and R.N. Fedorak. 1996. Increased permeability occurs in rat ileum following induction of pan-colitis. *Dig. Dis. Sci.* 41:405–411.

Diamond, J.M. 1977. Twenty-first Bowditch lecture. The epithelial junction: bridge, gate, and fence. *Physiologist.* 20:10–18.

Dragsten, P.R., R. Blumenthal, and J.S. Handler. 1981. Membrane asymmetry in epithelia: is the tight junction a barrier to diffusion in the plasma membrane? *Nature.* 294:718–722.

Fanning, A.S., and J.M. Anderson. 1996. Protein-protein interactions: PDZ domain networks. *Curr. Biol.* 6:1385–1388.

Farquhar, M.G., and G.E. Palade. 1963. Junctional complexes in various epithelia. *J. Cell Biol.* 17:375–412.

Fujimoto, K. 1995. Freeze-fracture replica electron microscopy combined with SDS digestion for cytochemical labeling of integral membrane proteins. Application to the immunogold labeling of intercellular junctional complexes. *J. Cell Sci.* 108:3443–3449.

Furuse, M., T. Hirase, M. Itoh, A. Nagafuchi, S. Yonemura, S. Tsukita, and S. Tsukita. 1993. Occludin: a novel integral membrane protein localizing at tight junctions. *J. Cell Biol.* 123:1777–1788.

Furuse, M., M. Itoh, T. Hirase, A. Nagafuchi, S. Yonemura, S. Tsukita, and S. Tsukita. 1994. Direct association of occludin with ZO-1 and its possible involvement in the localization of occludin at tight junctions. *J. Cell Biol.* 127:1617–1626.

Gossen, M., and H. Bujard. 1992. Tight control of gene expression in mammalian cells by tetracycline-responsive promoters. *Proc. Natl. Acad. Sci. USA.* 89:5547–5551.

Gumbiner, B., B. Stevenson, and A. Grimaldi. 1988. The role of the cell adhesion molecule uvomorulin in the formation and maintenance of the epithelial junctional complex. *J. Cell Biol.* 107:1575–1587.

Hall, A. 1998. Rho GTPases and the actin cytoskeleton. *Science.* 279:509–514.

Itoh, M., A. Nagafuchi, S. Yonemura, Y.T. Kitani, S. Tsukita, and S. Tsukita. 1993. The 220-kD protein colocalizing with cadherins in non-epithelial cells is identical to ZO-1, a tight junction-associated protein in epithelial cells: cDNA cloning and immunoelectron microscopy. *J. Cell Biol.* 121:491–502.

Janmey, P.A. 1994. Phosphoinositides and calcium as regulators of cellular actin assembly and disassembly. *Annu. Rev. Physiol.* 56:169–191.

Jesaitis, L.A., and D.A. Goodenough. 1994. Molecular characterization and tissue distribution of ZO-2, a tight junction protein homologous to ZO-1 and the *Drosophila* discs-large tumor suppressor protein. *J. Cell Biol.* 124:949–961.

Jou, T.-S., and W.J. Nelson. 1998. Effects of regulated expression of mutant RhoA and RacI small ATPases on the development of epithelial (MDCK) cell polarity. *J. Cell Biol.* 142:85–100.

Kimura, K., M. Ito, M. Amano, K. Chihara, Y. Fukata, M. Nakafuku, B. Yamamori, J. Feng, T. Nakano, K. Okawa, et al. 1996. Regulation of myosin phosphatase by Rho and Rho-associated kinase (Rho-kinase). *Science.* 273: 245–248.

Le Bivic, A., Y. Sambuy, A. Patzak, N. Patil, M. Chao, and E. Rodriguez-Boulan. 1991. An internal deletion in the cytoplasmic tail reverses the apical localization of human NGF receptor in transfected MDCK cells. *J. Cell Biol.* 115:607–618.

Lora, L., E. Mazzon, D. Martines, W. Fries, M. Muraca, A. Martin, A. d'Odorico, R. Naccarato, and S. Citi. 1997. Hepatocyte tight-junctional permeability is increased in rat experimental colitis. *Gastroenterology.* 113:1347–1354.

Luo, L., Y.J. Liao, L.Y. Jan, and Y.N. Jan. 1994. Distinct morphogenetic functions of similar small GTPases: Drosophila Drac1 is involved in axonal outgrowth and myoblast fusion. *Genes Dev.* 8: 1787–1802.

Madara, J.L. 1988. Tight junction dynamics: is paracellular transport regulated? *Cell.* 53:497–498.

Madara, J.L., D. Barenberg, and S. Carlson. 1986. Effects of cytochalasin D on occluding junctions of intestinal absorptive cells: further evidence that the cytoskeleton may influence paracellular permeability and junctional charge selectivity. *J. Cell Biol.* 102:2125–2136.

Madara, J.L., and K. Dharmsathaphorn. 1985. Occluding junction structure-function relationships in a cultured epithelial monolayer. *J. Cell Biol.* 101: 2124–2133.

Madara, J.L., J. Stafford, D. Barenberg, and S. Carlson. 1988. Functional coupling of tight junctions and microfilaments in T84 monolayers. *Am. J. Physiol.* 254:G416–G423.

Matsui, T., M. Maeda, Y. Doi, S. Yonemura, M. Amano, K. Kaibuchi, S. Tsukita, and S. Tsukita. 1998. Rho-Kinase phosphorylates COOH-terminal threonines of ezrin/radixin/moesin (ERM) proteins and regulates their head-to-tail association. *J. Cell Biol.* 140:647–657.

McCarthy, K.M., I.B. Skare, M.C. Stankewich, M. Furuse, S. Tsukita, R.A. Rogers, R.D. Lynch, and E.E. Schneeberger. 1996. Occludin is a functional component of the tight junction. *J. Cell Sci.* 109:2287–2298.

Nagafuchi, A., and M. Takeichi. 1988. Cell binding function of E-cadherin is regulated by the cytoplasmic domain. *EMBO (Eur. Mol. Biol. Organ.) J.* 7:3679–3684.

Nelson, W.J., and P.J. Veshnock. 1987. Modulation of fodrin (membrane skeleton) stability by cell-cell contact in Madin-Darby canine kidney epithelial cells. *J. Cell Biol.* 104:1527–1537.

Nusrat, A., M. Giry, J.R. Turner, S.P. Colgan, C.A. Parkos, D. Carnes, E. Lemichez, P. Boquet, and J.L. Madara. 1995. Rho protein regulates tight junctions and perijunctional actin organization in polarized epithelia. *Proc. Natl. Acad. Sci. USA.* 92:10629–10633.

Ridley, A.J., and A. Hall. 1992. The small GTP-binding protein rho regulates the assembly of focal adhesions and actin stress fibers in response to growth factors. *Cell.* 70:389–399.

Ridley, A.J., H.F. Paterson, C.L. Johnston, D. Diekmann, and A. Hall. 1992. The small GTP-binding protein rac regulates growth factor-induced membrane ruffling. *Cell.* 70:401–410.

Rodriguez-Boulan, E., and W.J. Nelson. 1989. Morphogenesis of the polarized epithelial cell phenotype. *Science.* 245:718–725.

Saitou, M., K. Fujimoto, Y. Doi, M. Itoh, T. Fujimoto, M. Furuse, H. Takano, and S. Tsukita. 1998. Occludin-deficient embryonic stem cells can differentiate into polarized epithelial cells bearing tight junctions. *J. Cell Biol.* 141:397–408.

Sekine, A., M. Fujiwara, and S. Narumiya. 1989. Asparagine residue in the rho gene product is the modification site for botulinum ADP-ribosyltransferase. *J. Biol. Chem.* 264:8602–8605.

Songyang, Z., A.S. Fanning, C. Fu, J. Xu, S.M. Marfatia, A.H. Chishti, A. Crompton, A.C. Chan, J.M. Anderson, and L.C. Cantley. 1997. Recognition of unique carboxyl-terminal motifs by distinct PDZ domains. *Science.* 275:73–77.

Staehelin, L.A. 1974. Structure and function of intercellular junctions. *Int. Rev. Cytol.* 39:191–284.

Stevenson, B.R., J.M. Anderson, D.A. Goodenough, and M.S. Mooseker. 1988. Tight junction structure and ZO-1 content are identical in two strains of Madin-Darby canine kidney cells which differ in transepithelial resistance. *J. Cell Biol.* 107:2401–2408.

Stowers, L., D. Yelon, L.J. Berg, and J. Chant. 1995. Regulation of the polarization of T cells toward antigen-presenting cells by Ras-related GTPase CDC42. *Proc. Natl. Acad. Sci. USA.* 92:5027–5031.

Takaishi, K., T. Sasaki, H. Kotani, H. Nishioka, and Y. Takai. 1997. Regulation of cell-cell adhesion by rac and rho small G proteins in MDCK cells. *J. Cell Biol.* 139:1047–1059.

van Itallie, C.M., and J.M. Anderson. 1997. Occludin confers adhesiveness when expressed in fibroblasts. *J. Cell Sci.* 110:1113–1121.

van Meer, G., B. Gumbiner, and K. Simons. 1986. The tight junction does not allow lipid molecules to diffuse from one epithelial cell to the next. *Nature.* 322:639–641.

van Meer, G., and K. Simons. 1986. The function of tight junctions in maintaining differences in lipid composition between the apical and the basolateral cell surface domains of MDCK cells. *EMBO (Eur. Mol. Biol. Organ.) J.* 5:1455–1464.

Willott, E., M.S. Balda, A.S. Fanning, B. Jamison, I.C. Van, and J.M. Anderson. 1993. The tight junction protein ZO-1 is homologous to the Drosophila discs-large tumor suppressor protein of septate junctions. *Proc. Natl. Acad. Sci. USA.* 90:7834–7838.

Wong, V., and B.M. Gumbiner. 1997. A synthetic peptide corresponding to the extracellular domain of occludin perturbs the tight junction permeability barrier. *J. Cell Biol.* 136:399–409.

Yeaman, C., A.H. Le Gall, A.N. Baldwin, L. Monlauzeur, A. Le Bivic, and E. Rodriguez-Boulan. 1997. The O-glycosylated stalk domain is required for apical sorting of neurotrophin receptors in polarized MDCK cells. *J. Cell Biol.* 139:929–940.